Active faulting and folding without topographic expression in an evaporite basin, Chile

T.E. Jordan†
Department of Earth and Atmospheric Sciences, Cornell University, Ithaca, New York 14853-1504, USA

N. Muñoz
SIPETROL (UK) Ltd., St. Andrew's House, Woking Surrey GU21 1EB, UK

M. Hein‡
T. Lowenstein
Department of Geological Sciences and Environmental Studies, Binghamton University, Binghamton, New York 13902, USA

L. Godfrey§
J. Yu
Department of Earth and Atmospheric Sciences, Cornell University, Ithaca, New York 14853-1504, USA

ABSTRACT

The Salar de Atacama in northern Chile accumulated halite during the Pliocene and Quaternary under conditions that alternated between a saline lake and a dry salt flat. Hidden beneath its uninterrupted flat surface is the Salar fault system. The halite deposits provide a high-resolution history of deformation. Contours on the ca. 5 Ma base of the halite unit in the southern salar, defined in a deep oil-exploration borehole and traced through reflection seismic lines, reveal that net reverse offset across the Salar fault system is down-to-the-east by ~900 m; of that total, 200 m occurred during the Quaternary and 700 m during the Pliocene. Distributions, thicknesses, and geometries of eight stratigraphic sequences within the halite unit reveal a history of episodic faulting and demonstrate that faulting during approximately half the 5 m.y. interval, including the Holocene, did not generate fault scarps. We suggest that deposition caused by evaporation of ground water brines in the salt flat, rather than either dissolution or deflation, has smoothed the topography of the dry lake bed across the active fault zone. For the case of west-directed groundwater flow, we propose that the east-facing Salar fault system focuses groundwater flux along the eastern flank of the fault, which enhances halite precipitation in the downthrown block during desiccated stages and counteracts fault-driven topographic relief. The realization that a seismic risk may exist even though the Salar fault system is hidden leads to the appreciation that similar unrecognized seismic risks may exist in more populous arid basins.

Keywords: active faults, Andes, geomorphology, halite, lakes, sequence stratigraphy.

INTRODUCTION

A commonly held assumption is that active faulting and folding creates vertical offset of the Earth's surface that calls attention to the youthfulness of the faults and folds (Keller and Pinter, 1996). Much of the geologic study that is the basis for earthquake-hazard assessment starts with mapping of the landform expressions of faults (Lettis et al., 1997). Indeed, in our northern Chilean study area, many Pliocene–Quaternary folds and faults have clear topographic expression, such as the Cordillera de la Sal (Fig. 1) (Jolley et al., 1990; Mpodozis et al., 2000). However, some faults are partially masked beneath anticlines, a condition referred to as a blind fault, although the fold is usually quite visible. The landform expression of the ongoing deformation may be reduced or eliminated by sediment accumulation on the flanks of, and even over the crest of, such a fold (Lettis et al., 1997). We present an extreme case of active faulting and folding with no topographic expression in the Salar de Atacama, Chile, which is an evaporite pan.

Lettis et al. (1997) investigated whether major reverse earthquakes are sometimes completely a surprise to well-trained Quaternary geologists where neither folds nor faults of Quaternary age are visible at the epicenter, a condition that geologists refer to as ''truly blind.'' Lettis et al. presented data for interplate zones (like Salar de Atacama) showing that ~90% of reverse earthquakes of magnitudes greater than Mw 5.9 occur along a Quaternary fault or fold that a geologist could have identified prior to the earthquake. The remaining 10% of such earthquakes occurred where geologic information is insufficient to judge seismic risk. Lettis et al. (1997) suggest that the remaining 10% of such earthquakes occurred where geological information is insufficient to judge seismic risk, but where surface deformation is probably recognizable. In contrast, they found that ~90% of intraplate earthquakes could not be detected by Quaternary geologists and are ''truly blind.''

Deposition adjacent to or across actively deforming structures is typically dominated by detrital sediments, fed from hills or mountains by hillslope processes and streams. But where stream systems terminate in closed basins and the climate is arid, evaporite deposits can constitute the syntectonic or ''growth'' strata. For

†E-mail: tej1@cornell.edu.
‡Present address: Department of Geology, Central Michigan University, Mount Pleasant, Michigan 48859, USA.
§Present address: Department of Earth and Environmental Sciences, Lehigh University, Bethlehem, Pennsylvania 18015, USA.

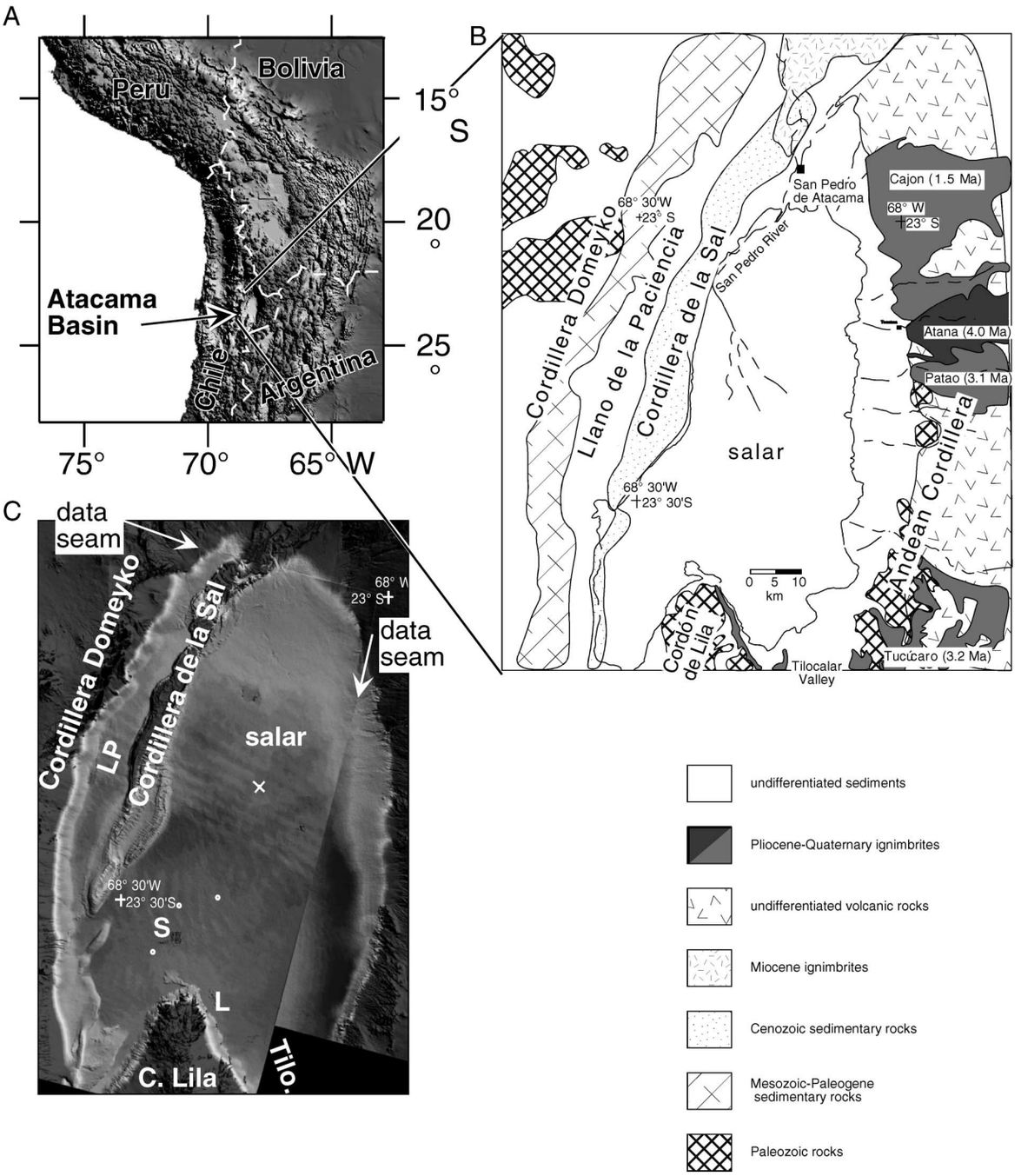

Figure 1. Digital elevation model (DEM) of the Andes Mountains and flanking lowlands, high-resolution DEM of Salar de Atacama in the Andean forearc, and drainage basin map. (A) Shaded elevation model of northern Chile, northwest Argentina, southern Peru, and southwest Bolivia, constructed from GTOPO5 data. The international border of Chile with Bolivia and Argentina approximates the position of the Andean volcanic arc. (B) Surface geology and drainage basin of Salar de Atacama, showing that the principal surface streams feeding the salar enter from the north and east. Geologic units from Ramírez and Gardeweg (1982). (C) A shaded DEM constructed from radar interferograms from successive passes of the European Space Agency radar satellite. Topographic scarps at margins of Cordillera Domeyko, Cordillera de la Sal, and Cordón de Lila are clearly defined, but no similar feature is visible within the desiccated salar. Gray scale is displayed such that very minor "ripples" are visible in the salar area and the seams between adjacent scenes are visible, to enhance even the slightest topographic features ("ripples" are due to contrasting atmospheric conditions between the two days of radar data acquisition). S—dark areas that are brine pools of SQM S.A.; L—brine pools of Sociedad Chilena de Litio S.A.; LP—Llano de la Paciencia; Tilo.—Tilocalar Valley. Also marked is the location of the petroleum exploration well ("X") that penetrated through the full halite unit, and three shallow boreholes (dots) studied in detail by Lowenstein et al. (2002) and Bobst et al. (2001).

the case described here, halite accumulation has masked all landform expression of faults and folds across which hundreds of meters of vertical offset occurred during the Pliocene and Quaternary. Tens of meters of offset during the Holocene created no topographic scarp, although high-resolution seismic reflection data reveal that scarps likely existed during certain intervals of the Pliocene–Pleistocene.

Deposition in this arid, closed-drainage basin occurs under two markedly different states. At times of relatively wetter climates, halite precipitates from concentrated brines in salt lakes. The deposition rate under these conditions is a function of volume and salinity of inflow water, evaporation rate, lake-water volume, and lake-water depth. At times of relatively drier climate (which prevails today), halite precipitates from the evaporation of groundwater brines at the upper surface of the groundwater system. That strata accumulate in this desiccated depositional environment is little appreciated (Lowenstein et al., 2002). In the Salar de Atacama, seismic reflection data reveal that the total thickness of halite locally reaches 1500 m, and a major fault traverses the center of the salar.

Here we document that a reverse fault zone, the Salar fault system, generated major vertical offset (~200 m locally) of the Salar de Atacama lacustrine strata during the Quaternary interval, including an estimated 15 m of vertical displacement during the 9000 yr span of human occupation of this region (Lynch and Stevenson, 1992). Furthermore, we demonstrate that a genetic relationship probably exists between the fault and the enhanced accumulation of halite on the downthrown fault block, which created the unusual situation of aggradation of a flat evaporite depositional surface that masks the potential seismic hazard.

PHYSIOGRAPHY AND GENERAL GEOLOGY OF SALAR DE ATACAMA

Salar de Atacama is a dry lake bed in the forearc of the Andes Mountains of northern Chile (centered near 23°30′S, 68°15′W) (Fig. 1). The Atacama basin lies within the Atacama desert, one of the driest deserts on Earth (Miller, 1976). The term *salar* refers to a desiccated lake covered with evaporite deposits.

Salar de Atacama, an essentially flat plain at 2300 m elevation in the bottom of a closed-drainage basin (the Atacama basin) (Fig. 1), receives detrital clastic sediments and water largely from the north and east. The flat plain is nearly 3000 km^2 in total area, composed of marginal zones of mixed siliciclastic, carbonate, and sulfate sediments (1300 km^2) and a central nucleus of nearly pure halite (1700 km^2) (Fig. 2), referred to in the literature as the halite nucleus (Moraga et al., 1974). The largest marginal sector (40 km × 30 km) forms the north end of the salar. Deposition in this northern marginal zone is controlled on the west by stream flow and groundwater from the Río San Pedro, which contributes siliciclastic detritus, and on the east by groundwater fed from streams entering from the east (Figs. 1B, 2A). The halite nucleus receives groundwater from aquifers, whose sources are in the Andean Cordillera to the east and southeast, and surplus from the northern marginal zone (Alonso and Risacher, 1996; Moraga et al., 1974; Bevacqua, 1991, 1995; Bevacqua and Chong, 1995). The halite nucleus is a highly irregular surface because it very rarely floods with surface water (Moraga et al., 1974); major sectors of the halite nucleus probably have not flooded for hundreds of years. The groundwater table is <1 m below the surface over the entire halite nucleus (Ide and Kunasz, 1989).

Mean precipitation (mostly summer rain) in the center of the salar is ~10 mm/yr. Greater precipitation falls on the Andean peaks north, south, and east of the Atacama basin, and stream flow and groundwater from those high-elevation zones supply the Salar de Atacama depositional system (Alonso and Risacher, 1996). Potential evaporation greatly exceeds surface-water input.

The Atacama closed basin is a peculiar topographic low perched on the western flank of the Andes (Fig. 1A). The Andean volcanic chain deflects to the east around the topographic low, whereas the western margin is confined by the Cordillera Domeyko, which exposes Paleozoic and Mesozoic rocks. The topographic basin is divided by a low but laterally continuous range, the Cordillera de la Sal, into a broad eastern sector, floored by the salar, and a narrow western sector, the Llano de la Paciencia (Fig. 1C). East of the salar, the Andean slope is underlain by latest Miocene and Pliocene ignimbrite volcanic rocks, which are buried near the salar margin by alluvial-fan deposits. Over most of the length of the salar, no topographic barriers separate the ignimbrites from the salar, so it is assumed that the ignimbrites continue in the subsurface of the salar. The Cordillera de la Sal exposes Oligocene–Pliocene strata that are strongly folded and faulted (Hartley et al., 1992; Flint et al., 1993; Naranjo et al., 1994; Muñoz et al., 1997; Mpodozis et al., 2000). Locally the eastern boundary of the Cordillera de la Sal is a fold hinge, implying continuity between the rocks that crop out in the Cordillera de la Sal and the subsurface of the salar. Likewise, seismic reflection profiles that cross the Cordillera de la Sal where it has minimum topographic relief reveal continuity of the folded strata into the subsurface of the salar. To the south, Paleozoic rocks of the Cordón de Lila range form a north-plunging anticline that protrudes as a peninsula into the halite nucleus. The ''embayment'' to the east of the peninsula, the Tilocalar Valley, is covered by ignimbrites and rises steadily southward in elevation to the volcanic centers of the Andes. A set of faults with Quaternary offset is well demonstrated to strike north to north-northwest through the Tilocalar Valley and Cordón de Lila peninsula (Niemeyer, 1984; Gardeweg and Ramirez, 1982), projecting toward Salar de Atacama (Fig. 2). These are moderate- to high-angle reverse faults (Kuhn, 1997). The ''embayment'' to the west of the peninsula rises southward over a divide near 3000 m toward another closed topographic basin, which holds the Salar de Punta Negra.

The Salar de Atacama formed in a large, unique low in the regional topography of the volcanic arc and forearc region (Isacks, 1988). The large dimensions of the low imply an origin that is at the scale of a major crustal or lithospheric feature. Deformation along the Salar fault system, on which this paper focuses, is probably an order of magnitude smaller than the offset on the feature(s) responsible for the Atacama basin. However, the Salar fault system may be one of a family of faults that, together, generated the Atacama basin. Faults west of Salar de Atacama (in the Cordillera de la Sal, the Llano de la Paciencia, and the Cordillera Domeyko) that had significant offset during the Miocene and Pliocene may be coupled to the Salar fault system (Muñoz et al., 2000).

Beyond the rugged small-scale relief of the halite crust (up to 1 m relief over horizontal distances of 1–2 m, caused by crystallization from groundwater), surface elevations of the Salar de Atacama show almost no variation. Even digital elevation models constructed from radar interferometry (vertical resolution 2–3 m) (Fig. 1C) reveal no scarps in the salar, although the data resolve a gradual decrease in elevation from the detrital clastic depositional systems of the northern marginal zone to the halite nucleus. The Salar fault system, discussed at length subsequently in this paper, does not have a topographic expression in the halite nucleus, which probably explains why the fault system does not appear on numerous geologic maps of the area (e.g., Ramírez and

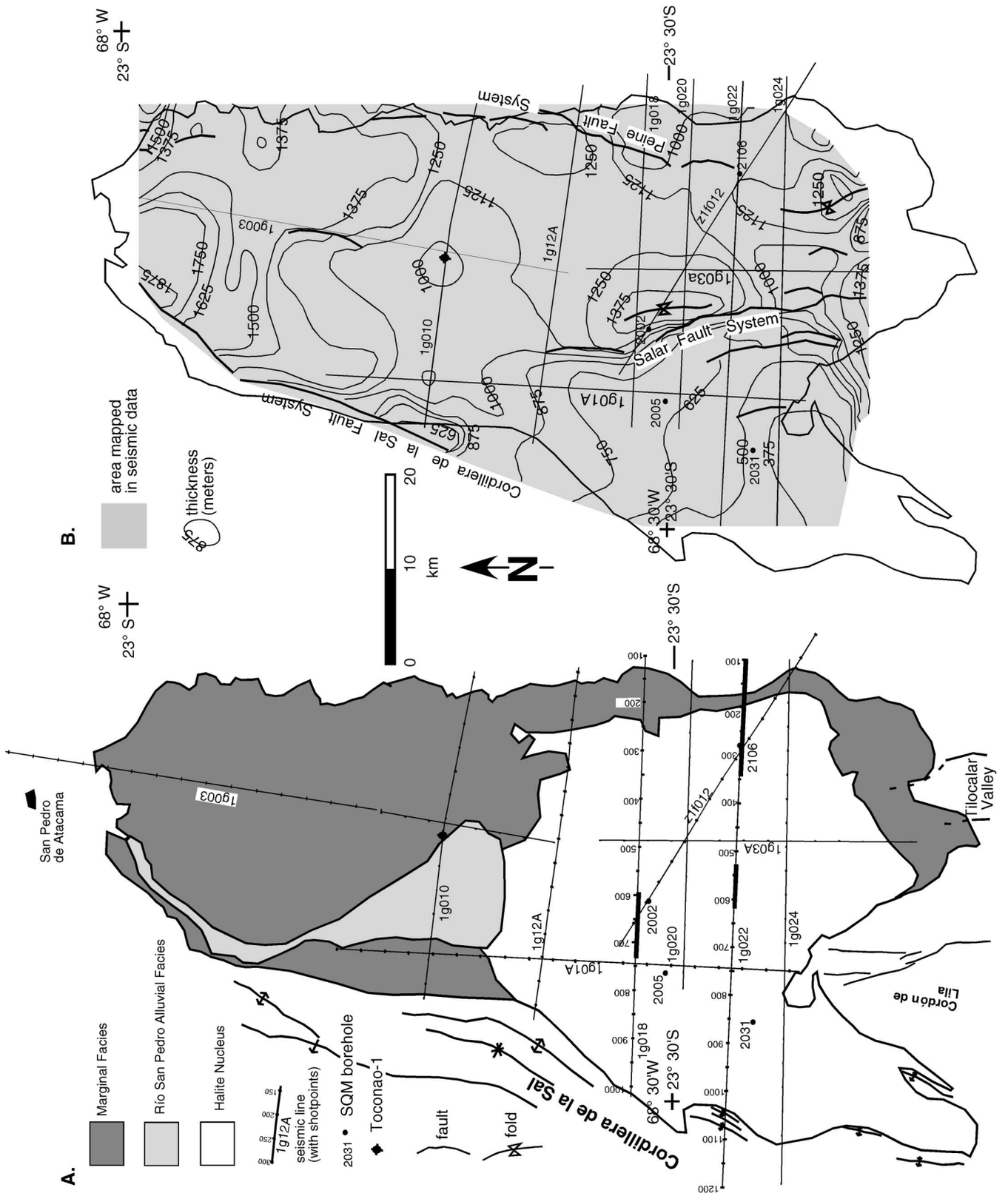
A.
B.
Marginal Facies
Río San Pedro Alluvial Facies
Halite Nucleus
seismic line (with shotpoints)
SQM borehole
Toconao-1
fault
fold
area mapped in seismic data
thickness (meters)
Cordillera de la Sal
Salar Fault System
Peine Fault System
San Pedro de Atacama
Tilocalar Valley
Cordón de Lila
68° W
23° S
23° 30'S
68° 30'W
0
10
20
km
N

Gardeweg, 1982). The only published report of the Salar fault system was the work of Flint et al. (1993), who studied the same seismic lines reported here. In contrast, in the southward extension of the Salar fault system beyond the salar, individual fault scarps in the Tilocalar Valley reveal several tens of meters to 200 m of offset of a 3.2 Ma ignimbrite (Gardeweg and Ramirez, 1982; Niemeyer, 1984). No folded strata adjacent to the fault system are visible in satellite images and aerial photographs of the salar, although folds are obvious in Thematic Mapper satellite images where the Cordillera de la Sal rises a few meters above the salar surface. Thus, Lettis et al. (1997) would classify the Salar fault system as a ''truly blind'' interplate reverse fault.

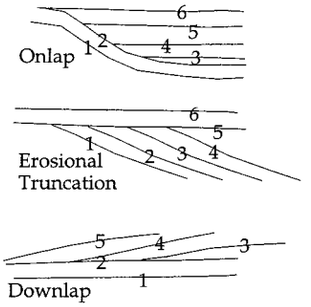

Figure 3. Terminology of the cross-sectional geometrical relationships between seismic reflections that are used to subdivide the strata into stratigraphic sequences and that lead to interpretations of topographic relief. The numbers signify temporal order.

SUBSURFACE DATA SETS AND MAJOR LITHOLOGIC PATTERNS

Empresa Nacional del Petróleo (ENAP) (Chile's national oil company) and its partners collected seismic reflection profiles over much of the Salar de Atacama for the purpose of oil exploration (Fig. 2A). The ~600 km of seismic lines consist of east-west–oriented profiles (spaced only 5 km apart in the halite nucleus and slightly farther apart in the northern marginal sector) and tie lines of north-south, northwest-southeast, and northeast-southwest orientations (spaced at variable intervals, typically 10–15 km apart). The depth to the base of the halite unit (980 m) was determined in the Toconao-1 well, which penetrated to 5 km depth adjacent to one of the seismic lines; data from this well allowed the conversion of seismic two-way traveltime (TWTT) to depth (Muñoz and Townsend, 1997). A second control point for depth conversion is the 356 m depth to a 6-m-thick ignimbrite (SQM S.A. borehole 2106, Fig. 2) which is visible as a strong reflection on seismic line 1g022.

For this paper, the seismic stratigraphy of the upper 1 s of TWTT of seismic data was studied in detail (lines shown in Fig. 2A) and extrapolated to fill the space between the seismic lines (gray area, Fig. 2B). The positions of unconformities within the halite unit were recognized on the basis of truncations and lapout relationships of reflections (Fig. 3); most of the geometrically defined sequence boundaries coincide with changes in rock properties registered in wireline log data for the Toconao-1 borehole. Each unconformable surface was traced among the multiple seismic lines to produce a complete description of the spatial extents of reflection packets bounded by unconformities and their conformable lateral equivalents, referred to as stratigraphic sequences (i.e., Cross and Lessenger, 1988). Eight stratigraphic sequences are distinguished within the halite unit (Figs. 4, 5). The thicknesses of the eight stratigraphic sequences (converted from TWTT to meters) were mapped by using a seismic interpretation work-station and then adjusted to remove artifacts created by boundaries of the data and irregular grid spacing.

Subsurface data were also provided by a set of 38 cores drilled in 1986 by a brine mining company, which is now the SQM Corporation. Bevacqua (1991) provided extensive descriptions of all the cores then available. Most of the cores were 30–40 m in length, but several of them penetrated several hundred meters. Core 2002, 500 m in length, achieved the deepest penetration. Core 2106, 390 m long, penetrated an ignimbrite along the eastern margin of the salar (Fig. 4), for which Bevacqua (1991) presented a K-Ar date that provides a key chronological constraint throughout the seismic grid. Bobst et al. (2001), Lowenstein et al. (2002), and Lowenstein et al. (2002) studied three of SQM's cores in detail (Figs. 2, 6) for paleoclimate reconstruction (cores 2031, 40 m long; 2005, 100 m long; the upper 200 m of 2002). The chronology of the most recent 325,000 yr is well defined by U-series dates of halite in these cores.

The boreholes show that halite is the dominant rock type below the Salar de Atacama to depths of many hundred meters. The Toconao-1 oil-exploration borehole penetrated a unit dominated by halite to a depth of 980 m. On the basis of drill cuttings and wireline logs, detrital clastic sediments are a significant component of that halite unit only from 480 to 620 m depth (Muñoz and Townsend, 1997). Lateral mapping of the halite unit through the seismic grid reveals that the halite unit is ~1200 m thick near borehole 2002, 1500 m thick in the center of the halite nucleus, and locally >1800 m thick (although perhaps not constituting a halite facies) near the north end of the salar (Fig. 2B). The 500-m-long borehole (2002) in the center of the salar consists of halite, very minor interbeds of gypsum, and a few horizons with a volcanic ash component (Bevacqua, 1991). Drilling of 2002 stopped before the base of the halite was reached.

AGE CONSTRAINTS

U-series dates of halite in SQM boreholes 2002 and 2005 set tight limits on the history of the late Quaternary deposition (Figs. 6, 7). For example, those dates and thicknesses reveal that the top 100 m thickness of halite in core 2002 corresponds to ~100 k.y. of accumulation (1 mm/yr accumulation rate) (Fig. 6). Accumulation of the next older interval of halite was not as rapid, as the age of halite at 200 m depth is 325 ± 48 ka (0.4 mm/yr accumulation rate between 100 and 200 m).

Another key chronological control on the salar deposits comes from SQM core 2106 (Figs. 2, 4), which sampled a 6-m-thick ignimbrite at 356 m depth in the southeast sector of the salar and then terminated after penetrating another 30 m of gypsum (Bevacqua, 1991) (Fig. 4). The K-Ar date for the ignimbrite, 3.1 ± 0.3 Ma, is very similar to ages of major ignimbrite sheets that crop out immediately to the east and south of the salar (Fig. 1B) (Bevacqua, 1991). These two ignimbrites, the 3.1 ± 0.2 Ma Patao and the 3.2 ± 0.7 Ma Tuc-

Figure 2. (A) Sedimentary domains of the modern salar. Stratigraphic study focused on the ENAP seismic lines shown, and shotpoint numbers are given for the lines used in Figure 5. Locations shown of cores studied by Bobst et al. (2001) and Lowenstein et al. (2002), of borehole 2106 that penetrated a 3.1 Ma ignimbrite, and of the Toconao-1 deep exploration borehole. (B) Thickness map (contours in meters) of the Pliocene–Quaternary halite unit. Gray pattern shows full spatial extent of the seismic grid on which the isopach maps are based. Segments of seismic lines illustrated in Figures 4 and 5 are shown as bold lines.

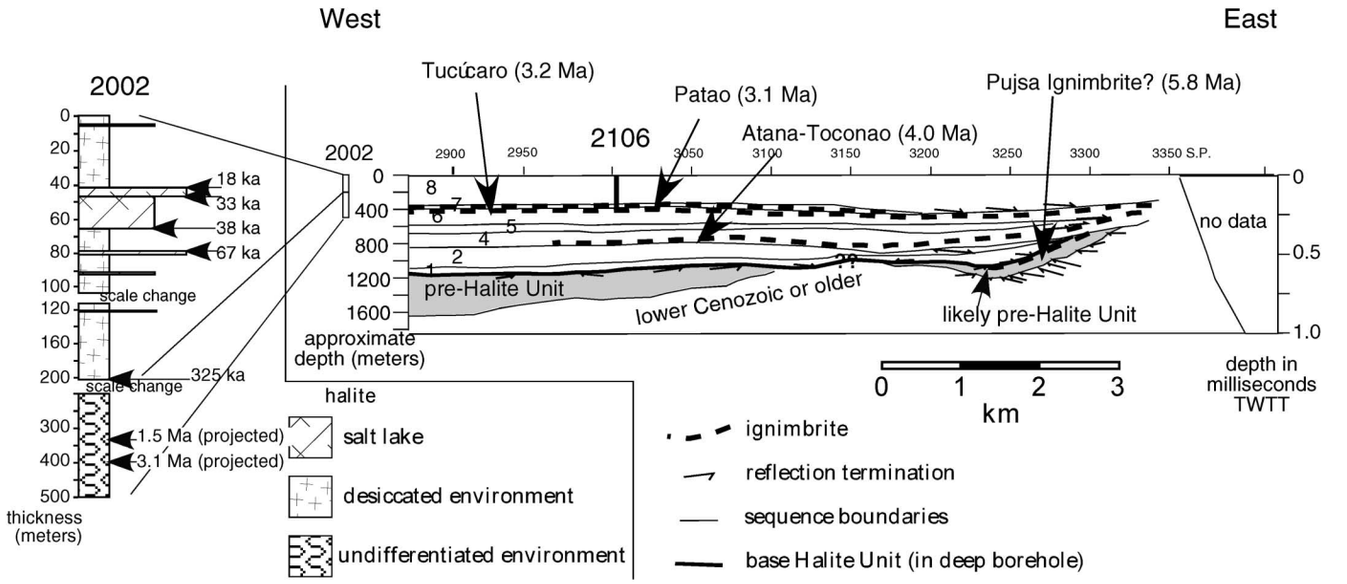

Figure 4. Principal chronologic constraints on the age of the halite unit. The cross section (eastern part of seismic line 1g022) has dimensions of horizontal position vs. TWTT (right axis) and shows sequence boundaries and reflections that are interpreted as ignimbrites. An approximate depth conversion is illustrated along the left axis. Borehole 2106 penetrates the uppermost ignimbrite, and its K-Ar age (3.1 Ma, Bevacqua, 1991) coincides with that of the Patao Ignimbrite. See text for explanation of the correlation of the sequence 4 strong reflection to the Atana-Toconao Ignimbrite. Borehole 2002, whose penetration depth is illustrated relative to the cross section, is located ~13 km northwest of the western margin of the cross section. The stratigraphic column at the left summarizes environmental interpretations as well as additional chronological information given by the U-series dates of halite in core 2002 (details in Fig. 6). Stratigraphic sequences are numbered near the west end of the cross section.

úcaro, were produced by two different eruptions (Ramírez and Gardeweg, 1982) and likely overlie one another in the subsurface. A prominent seismic reflection (trough) of low frequency and excellent lateral continuity occurs immediately below the two-way traveltime appropriate to the cored ignimbrite on the two seismic lines that pass within a few hundred meters of borehole 2106 (1g022 and Z1f012) (Fig. 2). Our interpretation that the prominent reflection is the seismic expression of the lower ignimbrite (Tucúcaro), which is likely thicker than the cored Patao Ignimbrite, provides a diagnostic tool for identifying other ignimbrites on the basis of similar seismic properties.

The total age of the halite unit is loosely defined by the extrapolation into the seismic lines of several other ignimbrites that are dated north and east of the salar. Near the east end of line 1g018, three very prominent reflections likely correspond to three ignimbrite-dominated horizons that crop out on the slopes east of the alluvial fans (Fig. 1B): The 3.1 Ma Patao Ignimbrite, the ca. 4.0 Ma Atana and Toconao Ignimbrites, and the 5.8 Ma Pujsa Ignimbrite (Ramírez and Gardeweg, 1982; Gardeweg and Ramírez, 1987; Lindsay et al., 2001). A conservative interpretation of seismic lines 1g018 and 1g022 is that the oldest ignimbrite underlies the base of the halite unit, placing the base of the halite unit younger than 5.8 Ma. However, the age of the oldest seismically defined ignimbrite in the eastern sector of the salar is poorly determined, with possibilities ranging from the 5.8 Ma Pujsa Ignimbrite to other ignimbrites with ages near 10 Ma that are known only in isolated outcrops (Lindsay et al., 2001). In addition, seismic sequence 4 likely contains one or more major ignimbrites, identified near the east ends of lines 1g010, 1g022, and 1g024, the south end of 1g03a, and in the northern half of line 1g003. Because the sequence 4 ignimbrite is thick and widespread in the east, southeast, and northeast sectors of the salar, we correlate it to the Atana Ignimbrite and Toconao Ignimbrite pair. The ca. 4.0 Ma Atana and Toconao Ignimbrites correspond to eruption of the La Pacana caldera, some 60 km east of the salar, for which surface exposures lead to the estimate that the eruption was one of the largest documented anywhere, ejecting ~2500 km³ of rock (Gardeweg and Ramírez, 1987; Lindsay et al., 2001). These interpretations of subsurface occurrences of Pliocene and Miocene ignimbrites indicate that the age of the base of the halite unit is earliest Pliocene and, therefore, seismic sequences 1 through 7 are coeval with the evolution of the caldera systems whose ignimbrites blanket the Andes east of the salar.

The age constraints reveal that the eight seismic sequences probably are not of equal duration and that sequence 8 was unusually long lasting (Fig. 7). Coincident with the top of the 3.1 Ma ignimbrite is the boundary between seismic sequences 8 and 7 (Fig. 4). The base of sequence 8 onlaps the top of sequence 7 both to the west (Figs. 5A, 7) and east (Figs. 4, 7) of borehole 2002, implying that 2002 is located in what was a topographic low at the time of initiation of sequence 8. The degree of onlap in the central part of the salar is more pronounced at the 7/8 boundary than across most of the underlying sequence boundaries, and the degree of hiatus across the 7/8 boundary increases to both the east and west of 2002 (Fig. 7). A marked change in seismic facies at the 7/8 boundary (see subsequent discussion) could be construed as evidence of a hiatus even in the topographic low. Further insight is provided by the interpretation that the 1.5 Ma Cajón Ignimbrite (Ramírez and Gardeweg, 1982; referred to as the Purico Ignimbrite by de Silva, 1989), tentatively identified at ~250 ms TWTT beneath the northernmost 20 km of

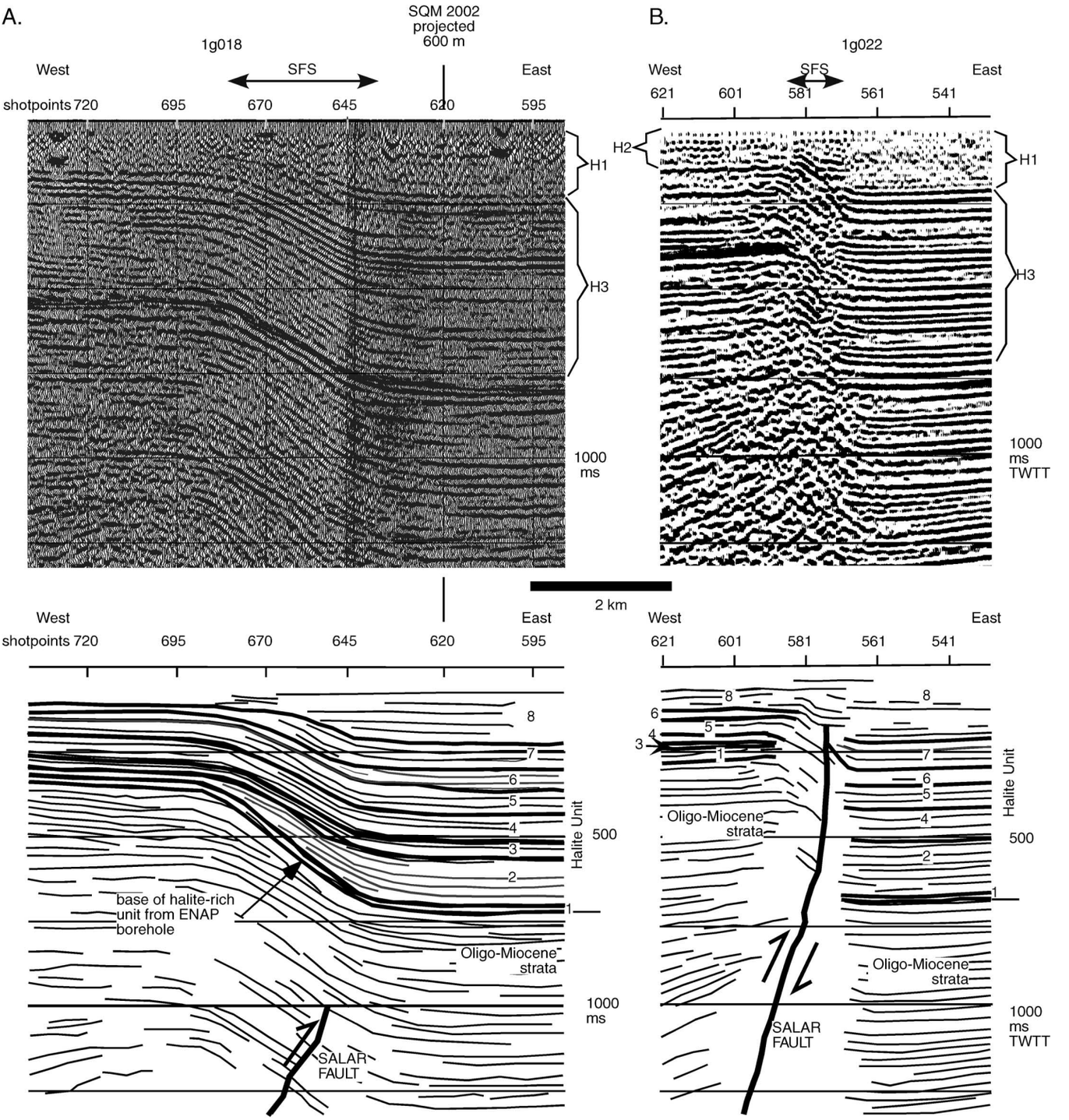

Figure 5. (Upper) Segments of seismic lines (A) 1g018 and (B) 1g022 near the Salar fault system (SFS). H1, H2, and H3 are seismic facies within the halite unit described in text. (Lower) The corresponding line drawings illustrate the eight stratigraphic sequences in the halite unit that are mapped on the basis of geometric criteria illustrated in Figure 3. Line locations shown in Figure 2. (A) Where crossed by 1g018, the tip of the Salar fault system is below the halite unit, which expresses the vertical offset as a monocline. (B) Where crossed by 1g022, the tip of the fault reaches the base of sequence 8.

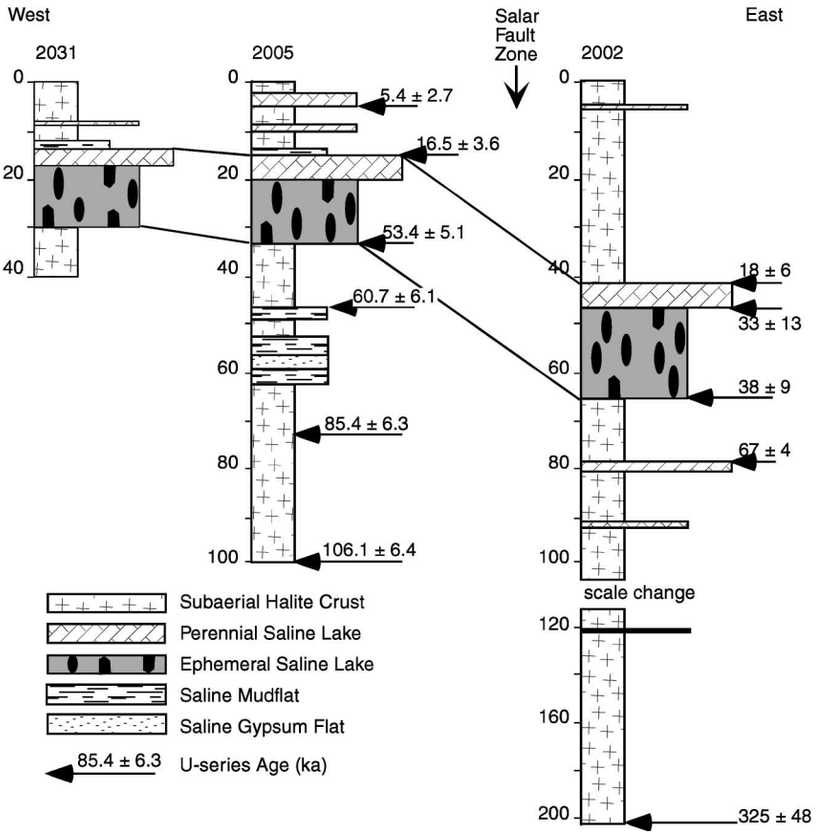

Figure 6. Summary of halite facies in sequence 8, documented in SQM cores. Boreholes 2031 and 2005 are located west of the Salar fault system, whereas borehole 2002 is located east of the Salar fault system (see Fig. 2). U-series dates from boreholes 2005 and 2002 and comparisons of halite depositional environments at the three sites allow temporal correlation among the cores. The top of the perennial saline lake facies, dated as ca. 16.5 ka, is readily identifiable in all three locations. That horizon occurs at similar depths in cores 2005 and 2031, but is vertically displaced ~28 m across the Salar fault system. From Lowenstein et al. (2002).

the salar on seismic line 1g003, traces through the seismic grid to a depth of ~330 m in SQM borehole 2002. Preservation of lower Pleistocene horizons implies either that accumulation was slow and steady across the sequence 7/8 boundary in the center of the halite nucleus or that a hiatus of duration ≤1 m.y. separates the two sequences. In summary, we interpret that sequence 8 approximates the Quaternary, whereas the salt in sequence 7 is of late Pliocene age (Fig. 7).

FACIES VARIATIONS IN THE HALITE UNIT

Throughout the late Quaternary, the depositional environments in the Salar de Atacama alternated between desiccated conditions (like those of today) and saline lake conditions (Lowenstein et al., 2002; Bobst et al., 2001). Both states resulted in accumulation of halite in the halite nucleus. Similarly, during the Pliocene, a saline closed-drainage system existed and generated a large volume of halite, though little is known about the depositional conditions.

The distribution of ignimbrites reflects lateral facies changes within the halite unit. For example, lateral tracing of the ignimbrite reflector penetrated in core 2106 through the seismic grid (Fig. 4) reveals that the 3.1 Ma horizon is near 390 m depth in core 2002, but no ignimbrite is intersected by core 2002 or borehole Toconao-1. At ~ 390 m depth, core 2002 reveals monotonous halite, and halite dominates to the end of the core at 500 m depth (unpublished report by P. Bevacqua to SQM S.A. in 1987; also, Bevacqua, 1991). Similarly, restriction of the prominent reflections that we consider to be diagnostic of ignimbrite to the southeast, east, and northeast margins of the seismic grid suggest that the ignimbrites interfinger toward the halite nucleus with salar evaporites.

Comparison of the borehole data to the seismic data reveals three different seismic facies of halite composition (Fig. 5). Although the lithology revealed in the 500 m thickness of core 2002 changes little with increasing depth, the seismic facies changes notably within the depth range that corresponds to core 2002. The upper 220 ms of line 1g018 is characteristically nonreflective (seismic facies H1). Below that depth, reflectivity increases. The division between the nonreflective and more reflective sectors occurs at the base of seismic sequence 8. With the exception of a pair of basal reflections, sequence 8 east of the Salar fault system throughout the southern and central halite nucleus corresponds to a very poorly reflective facies, whose few reflections are of high frequency (H1). West of the Salar fault system, in the northern part of the northern marginal zone, and near the eastern extreme of the halite nucleus, similar depths are moderately reflective (H2) (Fig. 5B, left side). Throughout the seismic grid shown in Figure 2A, the halite unit below sequence 8 is highly reflective (seismic facies H3) and has a lower frequency than typical of the seismic facies H1 and H2 (Fig. 5). Although the base of sequence 8 coincides with a facies change in part of the salar, boundaries between the seismic facies are not generally the same as the boundaries between stratigraphic sequences: sequence 8 comprises both facies H1 and H2, and sequences 1–7 display both facies H2 and H3.

The SQM cores and borehole Toconao-1 reveal that all three seismic facies are dominated by halite. It is likely that the greater reflectivity of sequence 8 (H2) west of the Salar fault system and in the marginal zones corresponds to a greater frequency of interbeds of gypsum and detrital clastics than exists within the halite nucleus east of the fault zone (e.g., Bevacqua, 1991). Core 2002 penetrates 110 m of seismic facies H3 and reveals no profound differences between rocks of seismic facies H1 compared to those of H3. But ignimbrites and detrital clastic rocks penetrated in the lower parts of the halite unit in boreholes 2106 and Toconao-1 reveal that the halite unit below sequence 8 interfingers with the volcaniclastic rocks and detrital sediments so evident in the geology to the north, east, and south of the salar (Bevacqua, 1991; Ramírez and Gardeweg, 1982). Drainage changes, gradient changes, and episodic supply of abundant fragmental debris associated with the eruptions could

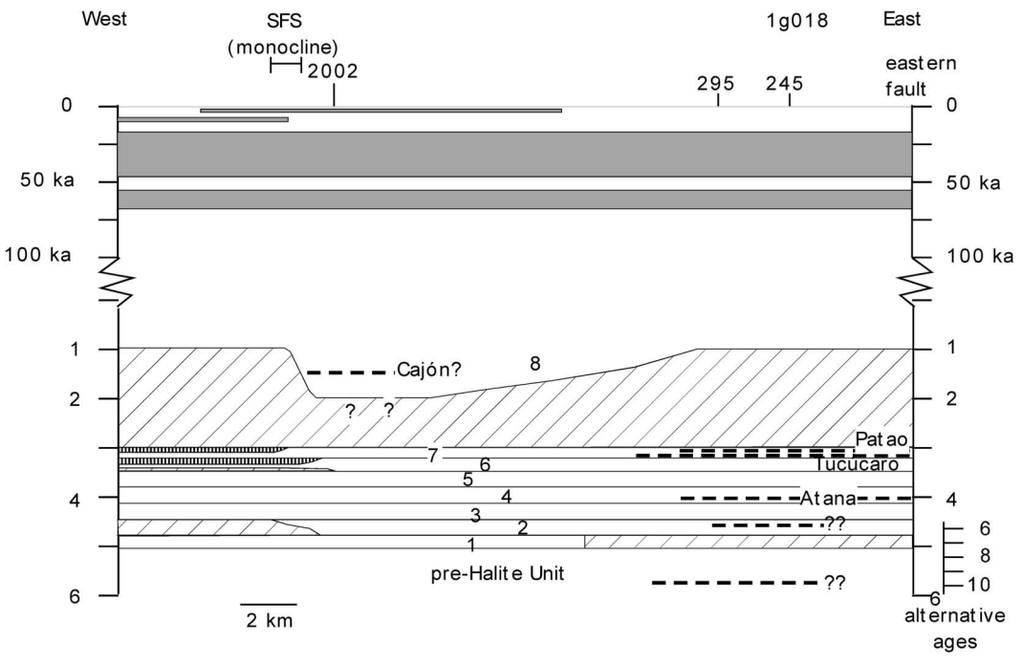

Figure 7. Chronostratigraphic (Wheeler) diagram of the halite unit in the southern part of the salar, constructed from seismic data (1g018) and borehole 2002. The time scale is determined from the ignimbrite and halite chronology summarized in Figure 4, plus the interpretation that the 1.5 Ma Cajón ignimbrite (exposed northeast of the salar, Fig. 1) occurs in sequence 8 of seismic line 1g003. The ages of the other stratigraphic sequences are assigned by spacing the undated sequences equally between the age-defined sequences. Note change in temporal scale, to allow greater resolution of the most recent 100 k.y. In the past 100 k.y., gray represents the distribution of saline lakes. Note also that poor constraints on the ages of interpreted ignimbrites in the deeper parts of the halite unit result in two general alternatives: The oldest three units span only the interval from 5 to 4 Ma, or they span much of the time between 10 and 4 Ma. Diagonal ruling indicates depositional hiatus; vertical ruling indicates likely removal, by erosion or dissolution.

readily be responsible for repeated changes in the Pliocene Salar de Atacama depositional system and be the root of strong reflectivity in H3.

FIDELITY OF THE STRATIGRAPHIC RECORD OF THE HALITE NUCLEUS

Stratal relationships across unconformities like those separating the eight stratigraphic sequences may be rich sources of information about deformation history (Suppe et al., 1992). But similar geometries may reflect steady landform change (for either tectonic or volcanic causes) between times of variable rates of accumulation of sediment or may indicate steady accumulation of sediment across a zone with episodic bursts of deformation or volcanism that would have changed surface gradients, drainage organization, and detrital sediment supply. Therefore, before applying the Salar de Atacama halite beds to an evaluation of the history of an active fault, it is important to determine the frequency at which stages of deformation are recorded in the strata, which can be termed the fidelity of the historical record (e.g., Sadler, 1981; Anders et al., 1987; Beer, 1990). Although lake deposits are considered in general to be excellent recorders of past environmental states, the completeness of a history captured in evaporite deposits is less certain. Uncertainty exists because evaporites form only under a small set of extreme climatic and hydrologic conditions and because they are subject to dissolution when those conditions change. In some salt basins, large percentages of preserved halite formed through dissolution and reprecipitation in the very shallow subsurface (top few meters to tens of meters) and do not reflect the conditions during surface deposition (Casas and Lowenstein, 1989).

What has been termed ''temporal completeness'' assesses the degree to which the preserved stratigraphic record at a single location samples steadily through time and can be quantified for a specified sampling frequency. What has been termed ''spatial completeness'' assesses the lateral continuity of strata that represent individual time increments and is useful to clarify whether strata from a single location contain as complete a record as could be achieved by integrating data over a large region. Lowenstein et al. (2002) demonstrated good spatial completeness of the upper Quaternary halite by showing that locations separated by tens of kilometers (cores 2031, 2005, and 2002, the latter two with U-series dates) record a similar sequence of variations in the environmental conditions at equal times during the past 100 k.y. (Fig. 6). The limitations to this spatial completeness are evident from the seismic stratigraphy.

One straightforward assessment implying that the halite nucleus record is temporally complete for a sampling frequency of ~3000 yr comes from recognition that a series of independently established latest Pleistocene and Holocene climate events, each ~3000 yr in duration, are recorded in the Atacama evaporite strata. Records from Chilean Andean lakes <100 km east of Salar de Atacama and vegetation history on the slopes east and south of the Salar de Atacama document several climate events: a latest Pleistocene to early Holocene wet interval (ca. 13,400–10,600 calendar yr B.P.), a major Holocene arid interval (ca. 10,000–7000 calendar yr B.P.), a middle Holocene wet interval (reported as either very brief near 6880 or spanning 7000–4000 calendar yr B.P.), and a final time of intense aridity (ca. 4000–0 calendar yr B.P.) (Geyh et al., 1999; Betancourt et al., 2000; Grosjean et al., 2001, their ^{14}C data corrected to calendar years by using M. Stuiver and P. Reimer's ''CALIB 4.3'' software available at http://www.depts.washington.edu/qil/). The alternations between arid and less arid climates are marked by the lakes recorded in core 2005 (Fig. 6) (Bobst et al., 2001). The shallow-saline-lake deposits between 9 and 10 m depth correlate to the latest Quaternary–early Holocene wet interval. The overlying desiccated-saline-flat facies (5.0–9.0 m depth) records the subse-

quent arid early Holocene interval. The U-series date of 5.4 ± 1.4 k.y. for halite of the ephemeral-saline-lake facies (5.0–2.7 m depth) correlates well with slightly wetter middle Holocene conditions. The capping desiccated-salt-pan facies formed during the final Holocene arid interval. Both desiccated and wet environmental states prove to be stratigraphically complete for near-millennial time intervals.

An alternative quantitative description of temporal completeness is generated from the ratio of the rates of long-term accumulation (R_L) to short-term accumulation (R_S), expressed as a percentage [(R_L/R_S) × 100] and specific to the duration of the short-term measurements (e.g., 100,000 year sampling interval) (Sadler, 1981; Anders et al., 1987; Beer, 1990). Rates of accumulation over short durations that are higher than over long durations imply that long lapses in accumulation (hiatuses) are interspersed with the brief times of rapid accumulation. If so, the record is incomplete and unsteady. For most depositional environments, short-term rates are several orders of magnitude higher than long-term rates, and accumulation is clearly unsteady (Sadler, 1981). However, for the past 100 k.y. in Salar de Atacama, similar mean rates of accumulation exist over both long and short durations (Fig. 8): for intervals of ≤5000 yr, mean rates of 1.1 mm/yr and 1.2 mm/yr were measured in core 2005 and core 2002, respectively; for intervals of 50 to 100 k.y., mean rates of 0.9 mm/yr and 0.8 mm/yr were measured in core 2005 and core 2002, respectively. This similarity implies comparatively steady accumulation (82% and 67% completeness in cores 2005 and 2002, respectively) at a 5000 yr sampling interval, rather like Anders et al. (1987) documented for pelagic accumulation. Although we have no age constraints for time intervals shorter than 1100 yr, the nearly order-of-magnitude variability of rates for measurement intervals shorter than 5000 yr (0.4 mm/yr to 2.9 mm/yr) (Fig. 8) may indicate that deposition in the halite nucleus is unsteady for sampling intervals of ≤1000 yr. Comparison of the short-term rates in core 2002 to the full interval studied in the SQM cores (325 k.y.) implies less (but still remarkable 50%) temporal completeness.

At the location of borehole 2002, estimated rates of early Quaternary and Pliocene accumulation (0.04–0.12 mm/yr) are much slower than for the upper Quaternary halite (Fig. 8). At the 100 k.y. sampling frequency (for which rates are ~0.5 mm/yr), sequence 7 and the lower part of sequence 8 are 10%–20% complete. A greater degree of unsteadiness is no surprise, given that intervals longer than several hundred thousand years sample across sequence boundaries (Fig. 7). In contrast to most of the sequences within the halite unit, which are largely conformable east of the Salar fault system, sequence 8 is widely discordant. It overlaps erosionally truncated horizons in the east-central, west-central, and southwest parts of the salar, as well as onlaps deformed beds in the monocline. In light of the regional extent of the unconformable relationships at the base of sequence 8, a significant hiatus is likely between sequences 7 and 8. Near borehole 2002 in the halite nucleus, the duration of the hiatus could be as long as ~1 m.y. (Fig. 7).

CROSS SECTIONS ACROSS THE SALAR FAULT AND STRUCTURES REVEALED BY THICKNESS MAPS

Depth to the base of the halite unit (Fig. 2B) serves as a structure-contour map for a horizon ca. 5 Ma in age. Throughout the halite nucleus and the northern marginal sector, the halite unit exceeds 500 m (300 ms TWTT) thickness. Zones of maximum thickness occur in the central halite nucleus, southeast halite nucleus (approaching the Tilocalar Valley), and at the extreme north end of the salar (Fig. 2B). Minimum thicknesses, <500 m, occur in the southwest corner of the salar. Localized structural highs occur in the south-central marginal zone (site of the Toconao-1 well) and southeast sector of the salar. The most abrupt change of halite-unit thickness occurs across the north-northwest–trending Salar fault system, in the south-central part of the salar. Across the Salar fault system, the halite-unit thickness changes abruptly from values of 625–750 m (370–440 ms TWTT) on the west to values of 900–1500 m (530–890 ms TWTT) on the east (Figs. 2B, 5). In the northern part of the salar, the thickness increases markedly toward the Cordillera de la Sal fault system, which is the western border of the basin.

The seismic data across the Salar fault system reveal an along-strike transition between two deformation styles (Fig. 5). The first style, a steep reverse fault, is illustrated by line 1g022 and neighboring parallel seismic lines, where the Salar fault system transects the Pliocene part of the halite unit (sequences 1–7) as a complete rupture, with no stratigraphic continuity across it. The lower quarter of sequence 8 onlaps an east-dipping surface at the trace of the fault. In the central section of sequence 8, strata flex across the fault position, forming a monoclinal fold. In the top quarter of sequence 8, the reflections are continuous and subhorizontal across the fault zone. The fault dips ~85° westward in the upper ~500 m (300 ms TWTT) and ~55° below that depth.

Displacement across the fault imaged by line 1g022 diminishes northward such that the upper ~3000 m (1000 ms TWTT) of strata form an east-facing monocline above the tip of the fault (seismic line 1g018 and neighboring lines) (Fig. 5). Horizons located east of the fold at depths between ~340 m (200 ms TWTT) and the base of the halite unit flex across the fault line. Layers between ~340 and 80 m (200–50 ms TWTT) onlap the top of sequence 7; those below 170 ms (290 m) both onlap and are eastward rotated. Strata shallower than 50 ms (~80 m) appear to be horizontal across the fault and fold zone at the resolution of the seismic data. The Salar fault system near lines 1g018 and z1f012 is monoclinal at shallow depths because it is a zone of transfer between en echelon major faults (Fig. 2B); the major faults are more typical of the profile at seismic line 1g022. The reverse fault that cores the monocline below 1000 ms TWTT dips moderately (44°) to the west.

SPATIAL AND TEMPORAL VARIABILITY OF OFFSET ON THE SALAR FAULT

Differences among the patterns of sediment accumulation of the eight stratigraphic sequences within the halite unit (isopach maps, Fig. 9) reveal an episodic history of faulting. In general, the thickness pattern reflects a mixture of sediment ponding in the preexisting topographic low, differential tectonic movement at faults, and volcanically induced deposition. Volcanic activity directly influenced the thickness pattern by the penetration of major ignimbrite sheets into the salar, which temporarily created extra stratal thickness and topographic relief but which later was onlapped by younger strata. Time intervals of significant tectonic offset produce patterns dominated by strong thickness changes across the Salar fault system, moderate thickness changes across a set of north-northeast–striking faults (Peine fault system) near the eastern margin of the salar, and tilting toward the Cordillera de la Sal fault system (Fig. 9B). In contrast, thickness variations resembling domes and hollows typify times with little offset of the Salar fault system (Fig. 9A).

The history of episodic reverse fault displacement across the Salar fault system throughout the Pliocene–Quaternary emerges from comparison of thicknesses of the eight stratigraphic sequences across the fault zone

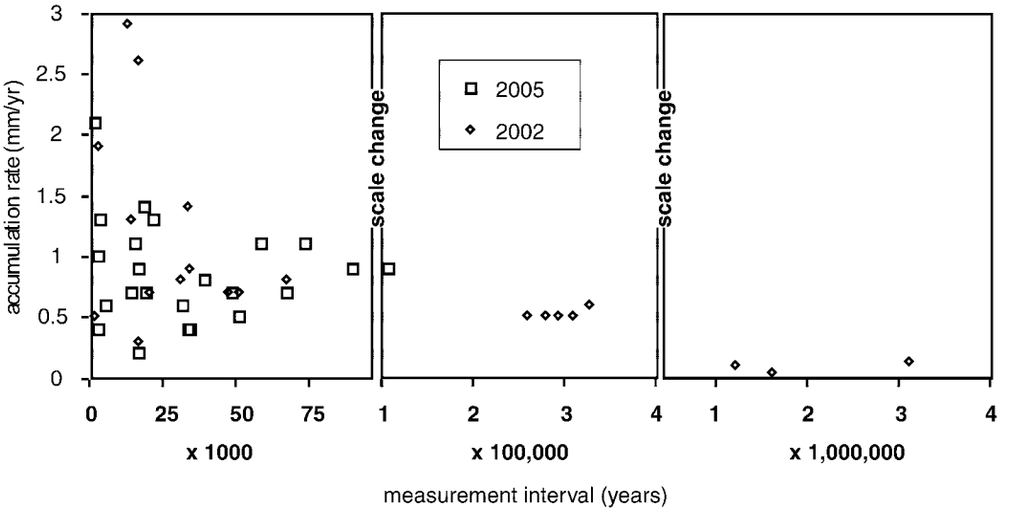

Figure 8. Graph of the variability of rates of accumulation in boreholes 2002 and 2005 (vertical axis) as a function of duration of the measurement interval (horizontal axis). Thicknesses and interval durations are derived from correlations illustrated in Figures 4, 6, and 7 and from correlations to independently dated climate events discussed in text. Note two changes in the scale of the horizontal axis.

in seismic lines 1g018 and 1g022 (Fig. 10A). Hundreds of meters of down-to-the-east displacement occurred during sequences 2, 7, and 8, but sequences 1 and 3 show little or no discernible offset in the north (1g018) and a few tens of meters of down-to-the-west displacement to the south (1g022). Displacement was variable during sequence 4 deposition and amounted to only tens of meters down-to-the-east during sequences 5 and 6. Examination of seismic lines that cross the Salar fault system at other locations underscores the lateral variability of the details of times of offset. Considered on a numerical time scale defined by ignimbrites, as previously described, the mean rate of reverse offset of the Salar fault system was higher during the Pliocene than during the Quaternary (Fig. 10B).

Intervals of onlap of strata in the fault zone indicate times when significant topographic relief was likely on the depositional surface of the salar. For most sedimentary rocks, truncation of the upper surface of already-deposited strata likewise would suggest the existence of a fault scarp, but the unique erosional possibilities of evaporite rocks might make a scarp unnecessary. Truncation in the absence of a scarp could occur if the halite dissolved downward to a horizontal plane controlled by low-salinity fresh water or groundwater. Where 1g018 crosses the Salar fault system, onlap onto an eastward-tilted surface is evident within sequence 2 and the lower part of 8; the top of sequence 7 is locally truncated. Sequence 6 appears to be truncated beneath 7 on the east flank of the Salar fault system. We interpret that topographic scarps likely existed at the times sequences 2 and 8 began to accumulate and may have formed during a hiatus between sequences 6 and 7. Where crossed by seismic line 1g022, only sequence 7 and the base of sequence 8 display onlap of a topographic feature in the Salar fault system zone. Truncation within the middle of sequence 8 implies a time of either erosion or dissolution at the fault zone. The truncation of the top of sequence 7 near the Salar fault system scarp and the onlap relationships of the base of sequence 8 in the Salar fault system zone are strong evidence that a fault scarp existed when sequence 8 began to accumulate. Also, fault scarps existed locally at two times of marked offset (Fig. 10) along the Salar fault system, during deposition of sequences 2 and 7. However, the paucity of evidence of fault scarps during roughly half of the Pliocene and Quaternary (e.g., today, during the latter part of sequence 8 deposition, and during deposition of sequences 4–6), despite hundreds of meters of tectonic offset, demonstrates that the depositional system of the halite nucleus is capable of masking active deformation along the Salar fault system beneath an unbroken surface.

SEISMIC RISK?

Keller and Pinter (1996) noted that the definition of an ''active'' fault or fold is imprecise, but is commonly taken to mean one that has undergone displacement during the time of human occupation. The Salar fault system is almost certainly active by that definition, irrespective of the lack of a surface topographic scarp. Whether it deforms seismically or aseismically is unknown.

Thickness variations of the halite unit indicate ~700 m of net down-to-the-east displacement since accumulation of the halite unit began. If we assume the base of the unit to be ca. 5 Ma, then the long-term vertical displacement rate on the Salar fault system is ~0.14 mm/yr. The oil-industry seismic data do not resolve the upper 100–200 m of the subsurface clearly enough to conclusively demonstrate that vertical fault displacement has cut or folded strata accumulated during the past 100 k.y. But the detailed stratigraphic and chronologic studies of 50, 100, and 200 m lengths of core remove the uncertainty: During the past 16.5 k.y., ~28 m more halite accumulated on the downthrown side of the fault than on the upthrown block (Lowenstein et al., 2002). This difference yields a vertical displacement rate of 1.7 mm/yr locally during the latest Pleistocene and Holocene, a rate that implies ~15 m of offset during the 9000 yr of human occupation of the region. Given the very low population density of the region, historical earthquakes may be poorly documented. Ongoing studies of shallow crustal seismicity in the region demonstrate that low-magnitude earthquakes (<2) occur in the crust beneath Salar de Atacama (A. Belmonte, 2001, personal commun.). On the basis of the criteria of Lettis et al. (1997), one would predict from the lack of any surface expression of the Salar fault system that the magnitude of its characteristic earthquake (the largest that occurs on a given fault) would be <6.0–6.4. However, this projection is based on a tiny data set (Lettis et al., 1997) and may not prove to be correct for this unusual depositional setting.

DEPOSITIONAL CONDITIONS CAPABLE OF ERASING SURFACE EXPRESSION OF FAULTING

On the basis of the fault history and depositional conditions, we suggest a model for to-

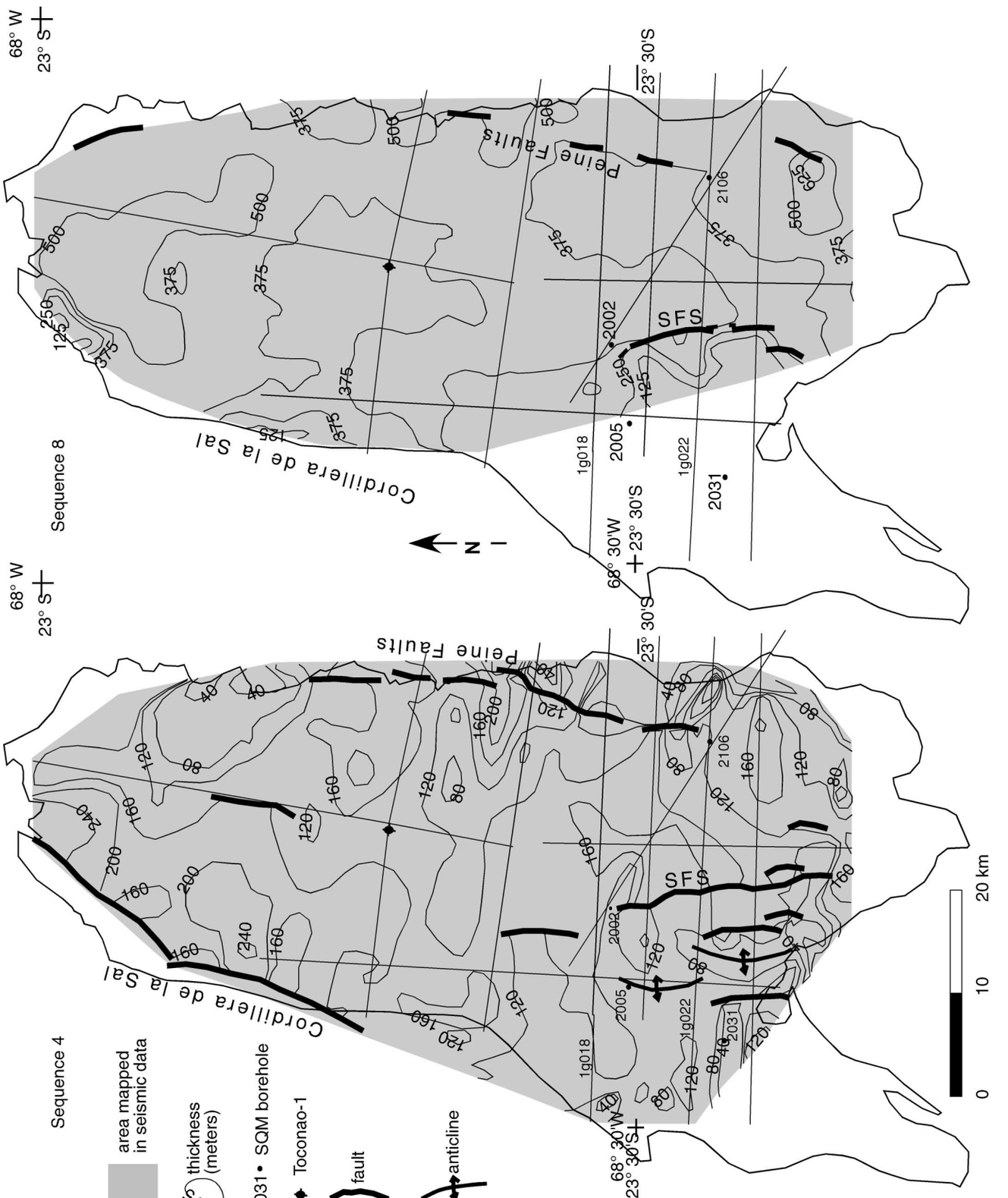
Sequence 8
Sequence 4
Cordillera de la Sal
Peine Faults
SFS
68° W
23° S
23° 30'S
68° 30'W
N
area mapped in seismic data
thickness (meters)
2031 • SQM borehole
Toconao-1
fault
anticline
0
10
20 km

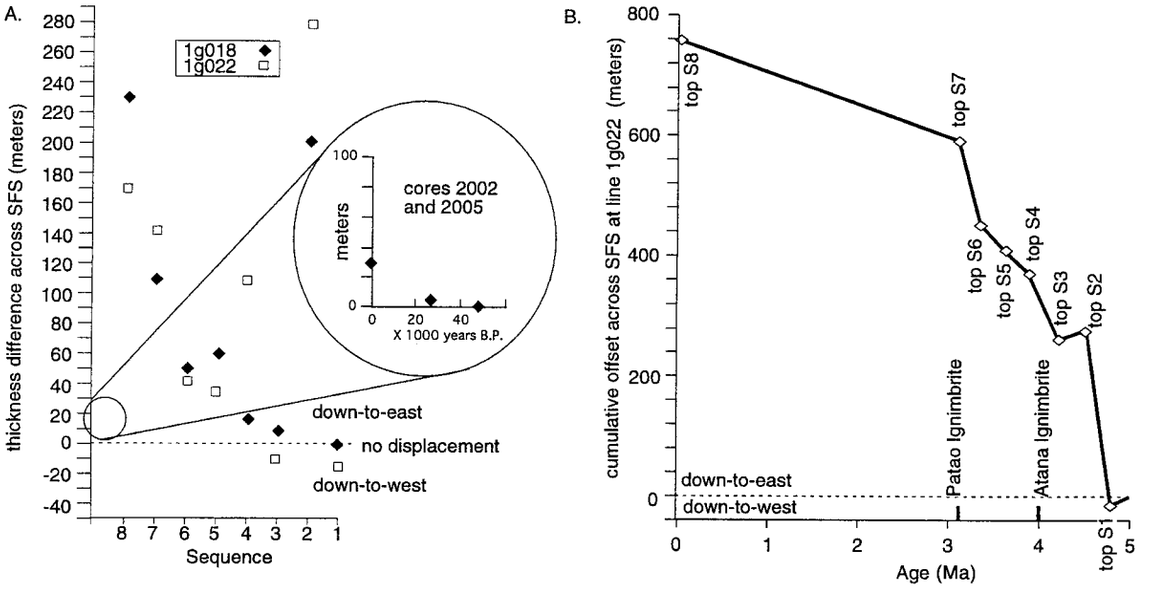

Figure 10. The incremental offset across the Salar fault system (SFS) varies markedly in different stratigraphic intervals. (A) As measured from seismic lines 1g018 and 1g022 (see Fig. 5), the difference in thickness of equivalent stratigraphic sequences on opposite sides of the Salar fault system measures the fault displacement during the time of that sequence. Times of maximum down-to-the-east reverse offset were during the deposition of sequences 2, 7, and 8 at both locations and sequence 4 near 1g022. Inset shows similar data for shorter time increments within sequence 8 (data illustrated in Fig. 6). (B) Cumulative offset of the Salar fault system where crossed by seismic line 1g022, constructed by summing the sequential offsets documented in A. Age assignments of the eight stratigraphic sequences in the halite unit follow Figure 7. The curve suggests that the long-term rate of reverse offset of the Salar fault system was higher between 5 and 3 Ma than it has been since 3 Ma.

pographic smoothing by deposition rather than erosion or dissolution in the halite nucleus. Halite deposition in the halite nucleus of Salar de Atacama occurs in three environments: in shallow saline lakes during times of wetter climate, by evaporation of groundwater in pore spaces in the first meter beneath the salar surface during desiccated times, and by diagenetic crystal growth in phreatic-zone pore spaces a considerable distance beneath the salar surface (Lowenstein et al., 2002; Bobst et al., 2001). The first two settings generate true aggradation of the sediment pile, thickening the column of rocks through time. The third mechanism probably increases the density of the strata through time, but does not aggrade thickness. Desiccated conditions existed for ~50% of the past 100 k.y. (Bobst et al., 2001) and 100% of the previous 200,000 yr (Lowenstein et al., 2002).

We estimate that during half of the Pliocene and Quaternary, rocks on opposing sides of the Salar fault system (and its associated fold) experienced relative vertical offset without creation of topographic relief. The lack of a fault scarp must be due to greater halite accumulation on the side of the downthrown structural block. At the scale of the upper 100 m of halite, comparison of the thickness of identical facies on opposing sides of the fault (core 2002 on the downthrown block and core 2005 on the upthrown block) shows differential accumulation during the desiccated-saline-flat conditions of the past 16.5 k.y., but the deposits of the previous saline-lake stage are of equal thickness in both locations. This result suggests an explanation that preferential accumulation on the downthrown fault block is coupled to a desiccated environment.

During desiccated climate states, groundwater-flow patterns dictate the supply of solutes to all locations in the salar. We hypothesize that the Salar fault system itself may be an important control on groundwater-flow paths. For water entering the salar from the alluvial fans on the east side, groundwater flow would be driven by the gravitational head of the west-sloping topographic surface such

Figure 9. Thickness maps (contours in meters) of two sequences. The thicknesses are derived from depth conversions of seismic data. Faults are mapped only where they cut the corresponding sequence at a scale detectable in the seismic data. (A) Sequence 4 illustrates a time interval during which displacement along the Salar fault system was subdued, and the pattern is dominated by a complex suite of domes and hollows that are a mixture of tectonic movement (note fold axes in the southwest sector of the salar and thickening toward the Cordillera de la Sal) and depositional relief on major volcanic units like the Atana Ignimbrite, which entered the salar from the east. (B) Sequence 8 illustrates a time interval during which thicknesses were controlled by the north-northwest–striking Salar fault system and a set of north-northeast–striking faults (Peine fault system) near the eastern margin of the salar. However, because some of the thickness change across the Salar fault system is due to filling of tectonic relief created during a hiatus following sequence 7 and some is expressed as monoclinal folding, sequence 8 is only locally cut by the Salar fault system. Continued offset along the Salar fault system at depth is confirmed by the differential offset at shallow depths (Fig. 6).

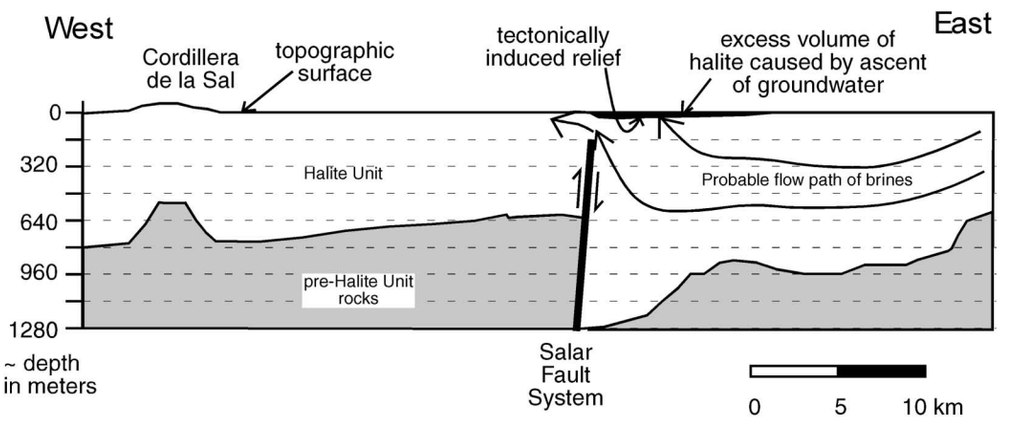

Figure 11. Cartoon illustrating a conceptual model of enhanced halite accumulation east of the Salar fault system, which leads to a horizontal depositional surface across the fault trace. Under the conditions of a desiccated surface environment, halite accumulates because of evaporation of groundwater-fed brines. A drop in permeability at the fault (either due to juxtaposition of lower-permeability rocks in the western fault block or due to properties of the fault zone itself) blocks the westward flow of topographically driven groundwater, forcing a high rate of upwelling in the downthrown eastern fault block.

that it flows subhorizontally toward the west (Fig. 11). Where that flow encounters the fault zone, if permeability is lower on the western fault block or in the fault zone, groundwater would be forced to ascend, causing near-vertical flow immediately east of the fault (Fig. 11). Given ample evaporation potential, the increased flux of water to the salar surface east of the fault would generate an increased rate of accumulation on the east side of the fault.

A permeability decrease at the fault could be caused either by contrasting properties of the rocks on the opposing sides of the fault or by fault-zone properties. Experience mining the brines in the Salar de Atacama clearly demonstrates that the halite is not dry, but rather that permeability and porosity in the upper tens of meters are high (6%–18%) (Alonso and Risacher, 1996) on both sides of the fault. At >4000 m depth beneath of the salar surface, a basement step (higher to west) of ~2000 m across the Salar fault system (a combined product of Cretaceous through late Cenozoic deformation) (Muñoz et al., 1997) could be responsible for a horizontal decrease in permeability toward the west. Equally plausible is that the fault zone itself is an impediment to horizontal groundwater flow. Rawling et al. (2001) described the effects of steeply dipping fault zones on groundwater flow and noted significant differences between the bulk permeability of fault zones in rocks that fracture brittlely and those in which the material flows rather than fractures. They concluded that large-displacement faults in nonfracturing rock types markedly impede horizontal flow, without substantially influencing vertical flow. The fact that halite flows rather than fractures indicates that the Salar fault system likely impedes horizontal flow, as illustrated in Figure 11. The subtle color variations in the region of the Salar fault system, visible in a Landsat TM image (bands 542), may be evidence of perturbed groundwater flow near the fault zone. Although the Peine fault zone also lacks fault scarps, this case of scarp elimination cannot be attributed as easily to groundwater-supplied differential halite accumulation because the fault zone occurs where volcaniclastic, siliciclastic, and evaporite depositional systems interfinger.

CONCLUSIONS AND IMPLICATIONS

The north-northwest–striking Salar fault system extends for at least 30 km through the Salar de Atacama, northern Chile, a desiccated lake in a hyperarid desert. The halite unit reveals at least 700 m of Pliocene–Quaternary down-to-the-east reverse motion across the fault in the southern sector of the salar, but locally the Salar fault system deforms the halite unit into a monocline with 400 m of structural relief. Rates of displacement throughout the Quaternary have been on the order of 0.1–2.0 mm/yr.

Despite large displacements and large displacement rates, no modern topographic scarp exists at the Salar fault system in the halite nucleus. Stratal geometries and thicknesses reveal variation between former times when there was a topographic scarp at the deformation zone and times with no topographic expression. The available borehole data suggest that both the times with and without a topographic scarp were likely dominated by halite accumulation adjacent to the Salar fault system.

We propose that the unique sedimentation processes in a groundwater-fed evaporite-generating environment are responsible for the lack of topographic expression of a major fault. During desiccated times, groundwater derived from topographically driven flow on the east side of the salar would have been forced upward by a barrier created at the fault zone, enhancing the supply of solutes to the zone immediately east of the fault (Fig. 11). This mechanism generates a higher rate of accumulation of halite east of the Salar fault system than to its west. The enhanced deposition on the eastern fault block is sufficient to prevent scarp formation during times of moderate displacement by the Salar fault system, though during times of especially high rates of offset, this depositional mechanism was not sufficient to prevent temporary formation of scarps.

Saline closed-lake basins are associated commonly with neotectonic (and potentially active) faults and folds. Similar settings exist in Death Valley, California, the Great Salt Lake, Utah, the Dead Sea Rift, and the Argentine Puna (Cemen et al., 1985; Galli, 1999; Jordan et al., 1999), to name a few. In a saline-lake environment, Dinter and Pechmann (1999) determined that a 3-m-high fault scarp accompanies a normal fault below the highly saline Great Salt Lake. For the East Great Salt Lake normal fault, the estimated 8 m offset during ~10,000 yr (J.C. Pechmann and D.A. Dinter, 2001, personal commun.) yields a displacement rate approximately half that of the Atacama case, so one cannot call on a slow

rate of offset of the Salar fault system as an explanation of its lack of topographic expression. The East Great Salt Lake fault scarp occurs at a depth of 5–10 m below the lake surface (Dinter and Pechmann 1999), similar to the maximum water depth of the Pleistocene saline lake in Atacama (Lowenstein et al., 2002). However, the Great Salt Lake differs from Atacama in that detrital clastic deposits accumulate during its deep-water phases, and halite only accumulated to significant thicknesses during its most desiccated states in local topographic lows adjacent to active faults (D.A. Dinter, 2001, personal commun.).

It is not yet known how common ''truly blind'' faults are in dry salt pans, but they are not unique to the Atacama basin. Perhaps similar to the Atacama basin, the Badwater salt flat of Death Valley is reportedly disturbed by only four short ($\leq$2.4 km) probable fault segments that are expressed as ''linear breaks'' but that have less relief than the irregular halite surface (Hunt and Mabey, 1966). Yet the Badwater salt flat occurs in a valley with abundant young fault scarps cutting alluvial-fan deposits on both flanks (e.g., Hunt and Mabey, 1966; Wright and Troxel, 1967; Wills, 1989; Blair, 1999). Perhaps the dearth of fault scarps in the salt pan is due to accretion of halite during the Quaternary (Lowenstein et al., 1999) rather than to lack of faults. In the Argentine Puna, a plateau region with multiple closed-drainage basins and abundant Quaternary and Neogene halite (Alonso et al., 1991), Quaternary deformation is widespread (Marrett et al., 1994). The Salar de Antofalla (centered at 25°47′S, 67°46′W) displays both folds in halite at the desiccated salar surface and faults between the salt pan and adjacent bedrock (Alonso et al., 1991) and was the location of a dominantly reverse-mechanism earthquake (Mb = 5.8) (Jordan et al., 1983; Chinn and Isacks, 1983). But at Salar de Hombre Muerto (25°20′S, 67°W) Quaternary faults within the area of halite accumulation lack faults scarps, folds, or juxtaposition of contrasting sediment types even though the faults can be inferred from gravity profiles, along-strike projections from visible faults, and aligned hot springs (Jordan et al., 1999).

Deposits of closed-lake basins, even saline deposits, are excellent recorders of local conditions. The high-fidelity Salar de Atacama halite deposits record a deformation history of a magnitude and style capable of generating earthquakes. Yet it is only the large-scale geometries of the strata that paint the fault history. The geomorphology of the modern salar is silent on the topic of faulting.

ACKNOWLEDGMENTS

We sincerely thank Carlos Herrero of ENAP and Carlos Nakousi of SQM for authorizing use of their data and for their encouragement. We are indebted to the National Science Foundation (grant ATM-9709771) and Fondo Nacional de Desarrollo Científico y Tecnológico (FONDECYT) (grant 1990009) for financial support. We thank our colleagues Lawrence Cathles and Richard Allmendinger (Cornell University), Andrew Bobst (Binghamton University), Constantino Mpodozis (Servicio Nacional de Geología y Minería [SERNAGEOMIN], Chile), and James Pechmann and David Dinter (University of Utah) for constructive conversations and Nicholas Pinter, Kirsten Menking, and Associate Editor Wanda Taylor for critical reviews of the manuscript.

REFERENCES CITED

Alonso, H., and Risacher, F., 1996, Geoquímica del Salar de Atacama: Parte 1. Origen de los componenets y balance salino: Revista Geológica de Chile, v. 23, p. 113–122.

Alonso, R.N., Jordan, T.E., Tabbutt, K.T., and Vandervoort, D., 1991, Giant evaporites of the Neogene central Andes: Geology, v. 19, p. 410–404.

Anders, M.H., Krueger, S.W., and Sadler, P.M., 1987, A new look at sedimentation rates and the completeness of the stratigraphic record: Journal of Geology, v. 95, p. 1–14.

Beer, J.A., 1990, Steady sedimentation and lithologic completeness, Bermejo basin, Argentina: Journal of Geology, v. 98, p. 501–517.

Betancourt, J.L., Latorre, C., Rech, J.A., Quade, J., and Rylander, K.A., 2000, A 22,000-year record of monsoonal precipitation from northern Chile's Atacama desert: Science, v. 289, p. 1542–1546.

Bevacqua, P., 1991, Geomorfologia del Salar de Atacama y estratigrafia de su nucleo y delta, segunda region de Antofagasta, Chile [Geomorphology of the Salar de Atacama, and stratigraphy of the nucleus and delta, Second region of Antofagasta, Chile] [master's thesis]: Antofagasta, Chile, Universidad Catholica del Norte, 284 p.

Bevacqua, P., 1995, Lacustrine deposits in the Preandean Atacama basin: The Salar de Atacama: GLOPALS-IAS Meeting, Excursion Guidebook, Antofagasta, Chile: Antofagasta, Chile, Universidad Católica del Norte, p. 47–62.

Bevacqua, P., and Chong, D., G., 1995, The Salar de Atacama of northern Chile: Evolution and stratigraphy of its nucleus: Antofagasta, Chile, GLOPALS-IAS Meeting Abstracts, p. 21–22.

Blair, T.C., 1999, Sedimentology of the debris-flow-dominated Warm Spring Canyon alluvial fan, Death Valley, California: Sedimentology, v. 46, p. 941–965.

Bobst, A.L., Lowenstein, T.K., Jordan, T.E., Godfrey, L.V., Hein, M.C., Ku, T.-L., and Luo, S., 2001, A 106 ka paleoclimate record from the Salar de Atacama, northern Chile: Palaeogeography, Palaeoclimatology, Palaeoecology, v. 173, p. 21–42.

Casas, E., and Lowenstein, T.K., 1989, Diagenesis of saline pan halite: Comparison of petrographic features of modern, Quaternary, and Permian halites: Journal of Sedimentary Petrology, v. 59, p. 724–739.

Cemen, I., Wright, L.A., Drake, R.E., and Johnson, F.C., 1985, Cenozoic sedimentation and sequence of deformational events at the southeastern end of the Furnace Creek strike-slip fault zone, Death Valley region, California, *in* Christie-Blick, N., and Biddle, K.T., eds., Strike-slip deformation, basin formation, and sedimentation: Society of Economic Paleontologists and Mineralogists Special Publication 37, p. 127–141.

Chinn, D.S., and Isacks, B.L., 1983, Accurate source depths and focal mechanisms of shallow earthquakes in western South America and in the New Hebrides island arc: Tectonics, v. 2, p. 529–563.

Cross, T.A., and Lessenger, M., 1988, Seismic stratigraphy: Annual Review of Earth and Planetary Sciences, v. 16, p. 319–354.

de Silva, S., 1989, Geochronology and stratigraphy of the ignimbrites from the 21°30′S to 23°30′S portion of the central Andes of northern Chile: Journal Volcanology and Geothermal Research, v. 37, p. 93–131.

Dinter, D.A., and Pechmann, J.C., 1999, Multiple Holocene earthquakes on the East Great Salt Lake fault, Utah: Evidence from high-resolution seismic reflection data: Eos (Transactions, American Geophysical Union), v. 80, p. F734.

Flint, S., Turner, P., Jolley, E.J., and Hartley, A.J., 1993, Extensional tectonics in convergent margin basins: An example from the Salar de Atacama, Chilean Andes: Geological Society of America Bulletin, v. 105, p. 603–617.

Galli, P., 1999, Active tectonics along the Wadi Araba–Jordan Valley transform fault: Journal of Geophysical Research, v. 104, p. 2777–2796.

Gardeweg, P., M., and Ramírez, R., C.F., 1982, Geología de los volcanes del Callejón de Tilocalar, Cordillera de los Andes—Antofagasta: III Congreso Geológico Chileno: Concepción, Chile, Universidad de Concepción, p. A111–A123.

Gardeweg, M., and Ramírez, C.F., 1987, La Pacana caldera and the Atana Ignimbrite—A major ash-flow and resurgent caldera complex in the Andes of northern Chile: Bulletin of Volcanology, v. 49, p. 547–566.

Geyh, M.A., Grosjean, M., Nunez, L., Schotterer, U., 1999, Radiocarbon reservoir effect and the timing of the late-glacial/early Holocene humid phase in the Atacama desert (northern Chile): Quaternary Research, v. 52, p. 143–153.

Grosjean, M., van Leeuwen, J.F.N., van der Knaap, W.O., Geyh, M.A., Ammann, B., Tanner, W., Messerli, B., Nunez, L.A., Valero-Garces, B.L., and Veit, H., 2001, A 22,000 ^{14}C year BP sediment and pollen record of climate change from Laguna Miscanti (23 degrees S), northern Chile, *in* Fard, A.M., ed., Recognition of abrupt climate changes in clastic sedimentary environments: Global and Planetary Change, v. 28, p. 35–51.

Hartley, A.J., Flint, S., Turner, P., and Jolley, E.J., 1992, Tectonic controls on the development of a semiarid, alluvial basin as reflected in the stratigraphy of the Purilactis Group (Upper Cretaceous–Eocene), northern Chile: Journal of South American Earth Sciences, v. 5, p. 275–296.

Hunt, C.B., and Mabey, D.R., 1966, Stratigraphy and structure, Death Valley, California: U.S. Geological Survey Professional Paper 494-A, 162 p.

Ide, Y., F., and Kunasz, I.A., 1989, Origin of lithium in Salar de Atacama, northern Chile, *in* Erickson, G.E., Cañas Pinochet, M.T., and Reinemund, J.A., eds., Geology of the Andes and its relation to hydrocarbon and mineral resources: Houston, Texas, Circum-Pacific Council for Energy and Mineral Resources, Earth Science Series, v. 11, p. 165–172.

Isacks, B.L., 1988, Uplift of the central Andean plateau and bending of the Bolivian orocline: Journal of Geophysical Research, v. 93, p. 3211–3231.

Jolley, E.J., Turner, P., Williams, G.D., Hartley, A., and Flint, S., 1990, Sedimentological response of an alluvial system to Neogene thrust tectonics, Atacama desert, northern Chile: Geological Society [London] Journal, v. 147, p. 769–784.

Jordan, T.E., Isacks, B.L., Allmendinger, R.W., Brewer, J.A., Ramos, V.A., and Ando, C.J., 1983, Andean tectonics related to geometry of subducted Nazca plate: Geological Society of America Bulletin, v. 94, p. 341–361.

Jordan, T.E., Alonso, R.N., and Godfrey, L.V., 1999, Tectónica, subsidencia y aguas en el Salar del Hombre Muerto, Puna, Argentina: XIV Congreso Geológico Argentino, Actas I, p. 254–256.

Keller, E.A., and Pinter, N., 1996, Active tectonics: Englewood Cliffs, New Jersey, Prentice-Hall, 337 p.

Kuhn, D., 1997, Deformationsanalyse der Salar de Atacama region (nordchile) und interpretation des neotektonischen Spannungsfelds (Ph.D. thesis): Berlin, Germany, Technical University, 133 p.

Lettis, W.R., Wells, D.L., and Baldwin, J.N., 1997, Empirical observations regarding reverse earthquakes, blind

thrust faults, and Quaternary deformation: Are blind thrust faults truly blind?: Seismological Society of America Bulletin, v. 87, p. 1171–1198.

Lindsay, J.M., de Silva, S., Trumbull, R., Emmermann, R., and Wemmer, K., 2001, La Pacana caldera, n. Chile: A reevaluation of the stratigraphy and volcanology of one of the world's largest resurgent calderas: Journal Volcanology and Geothermal Research, v. 106, p. 145–173.

Lowenstein, T.K., Hein, M.C., Bobst, A.L., Jordan, T.E., Ku, T.-L., and Luo, S., 2002, An assessment of stratigraphic completeness in climate-sensitive closed-basin lake sediments: Salar de Atacama, Chile: Journal of Sedimentary Research (in press).

Lowenstein, T.K., Li, J., Brown, C., Roberts, S.M., Ku, T.-L., Luo, S., and Yang, W., 1999, 200 k.y. paleoclimate record from Death Valley salt core: Geology, v. 27, p. 3–6.

Lynch, T.F., and Stevenson, C.M., 1992, Obsidian hydration dating and temperature controls in the Punta Negra region of northern Chile: Quaternary Research, v. 37, p. 117–124.

Marrett, R.A., Allmendinger, R.W., Alonso, R.N., and Drake, R.E., 1994, Late Cenozoic tectonic evolution of the Puna plateau and adjacent foreland, northwestern Argentine Andes: Journal of South American Earth Sciences, v. 7, p. 179–207.

Miller, A., 1976, The climate of Chile, *in* Schwerdtfeger, W., ed., Climates of Central and South America: Amsterdam, Elsevier Scientific Publishing Company, p. 113–145.

Moraga, A., Chong, G., Fortt, M.A., and Henriquez, H., 1974, Estudio geológico del Salar de Atacama, Provincia de Antofagasta: Instituto Investigaciones Geológicas, Boletín 29, 56 p.

Mpodozis, C., Blanco, N., Jordan, T.E., and Gardeweg, M.C., 2000, Estratigrafía, eventos tectónicos y deformación del Cenozoico tardío en la región norte de la cuenca del Salar de Atacama: La zona de Vilama-Pampa Vizcachitas: IX Congreso Geológico Chileno (Puerto Varas, Chile): Santiago, Sociedad Geológica de Chile, v. 2, p. 598–603.

Muñoz, N., and Townsend, G.F., 1997, Estratigrafía de la cuenca Salar de Atacama. Resultados del pozo exploratorio Toconao: 1. Implicancias regionales: VIII Congreso Geológico Chileno: Antofagasta, Chile, Universidad Católica del Norte, v. 1, p. 555–558.

Muñoz, N., Charrier, G., R., and Reutter, K.J., 1997, Evolución de la cuenca Salar de Atacama: Inversión tectónica y relleno de una cuenca de antepaís de retroarco: VIII Congreso Geológico Chileno: Antofagasta, Chile, Universidad Católica del Norte, v. 1, p. 195–199.

Muñoz, N., Charrier, R., and Radic, J.P., 2000, Formación de la Cordillera de la Sal por propoagación de fallas y plegamiento por despegue, II Región, Chile: IX Congreso Geológico Chileno (Puerto Varas, Chile): Santiago, Sociedad Geológica de Chile, v. 2, p. 604–608.

Naranjo, J.A., Ramírez, C.F., and Paskoff, R., 1994, Morphostratigraphic evolution of the northwestern margin of the Salar de Atacama basin (23°S–68°W): Revista Geológica de Chile, v. 21, p. 91–103.

Niemeyer R.H., 1984, La megafalla Tucúcaro en el extremo sur del Salar de Atacama: Una antigua zona de cizalle reactivada en el cenozoico: Santiago, Universidad de Chile, Departamento de Geología, Comunicaciones, no. 34, p. 37–45.

Ramírez, C., and Gardeweg, M., 1982, Hoja Toconao, Región de Antofagasta: Servicio Nacional de Geología y Minería, Carta Geológica de Chile, no. 54, 122 p.

Rawling, G.C., Goodwin, L.B., and Wilson, J.L., 2001, Internal architecture, permeability structure, and hydrologic significance of contrasting fault-zone types: Geology, v. 29, p. 43–46.

Sadler, P.M., 1981, Sediment accumulation rates and the completeness of the stratigraphic record: Journal of Geology, v. 89, p. 569–584.

Suppe, J., Chou, G.T., and Hook, S.C., 1992, Rates of folding and faulting determined from growth strata, *in* McKlay, K.R., ed., Thrust tectonics: New York, Chapman Hall, p. 105–121.

Wills, C.J., 1989, A neotectonic tour of the Death Valley fault zone, Inyo County: California Geology, v. 42, p. 195–200.

Wright, L.A., and Troxel, B.W., 1967, Limitations on right-lateral, strike-slip displacement, Death Valley and Furnace Creek fault zones, California: Geological Society of America Bulletin, v. 78, p. 933–949.

MANUSCRIPT RECEIVED BY THE SOCIETY 20 JULY 2001
REVISED MANUSCRIPT RECEIVED 23 APRIL 2001
MANUSCRIPT ACCEPTED 9 MAY 2002

Printed in the USA